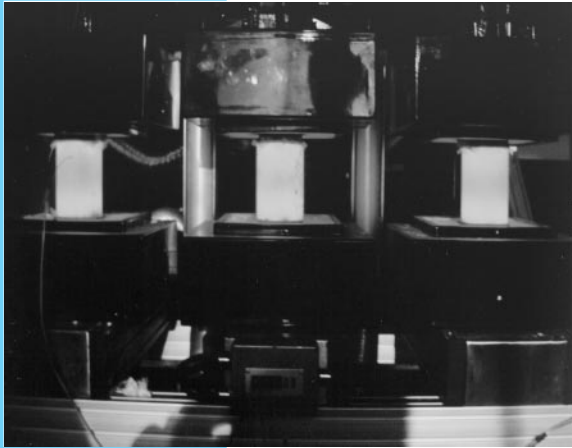


CHAPTER 18

Magnetic Materials



Each of these steel billets is being heated uniformly in a cost-effective way by two adjacent coils which utilize an oscillating electrical current to produce an oscillating magnetic flux and the resulting heating due to the “hysteresis” of a ferromagnetic core material. (Courtesy of CoreFlux Heating Systems.)

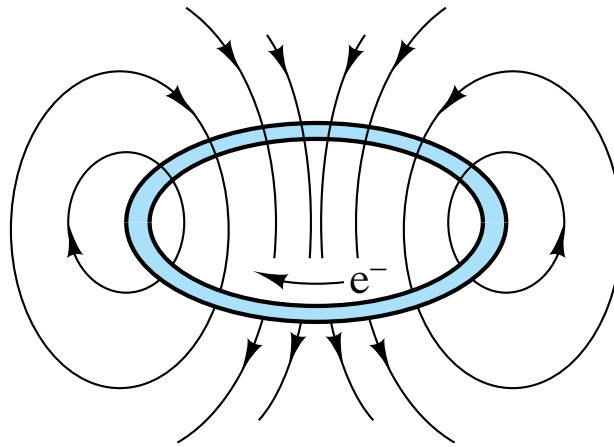


Figure 18-1 *A simple illustration of magnetism shows the magnetic field (seen as magnetic flux lines) generated around an electrical current loop.*

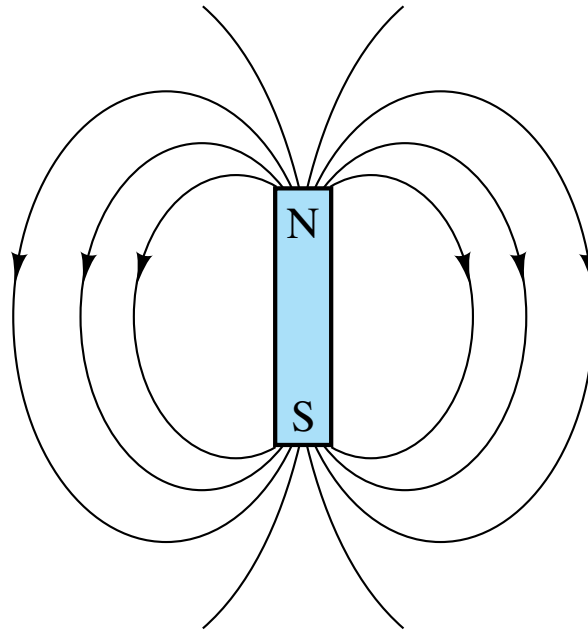


Figure 18-2 *A magnetic material can generate a magnetic field without an electrical current. This simple bar magnet is an example.*



Figure 18-3 *Attraction of two adjacent bar magnets.*

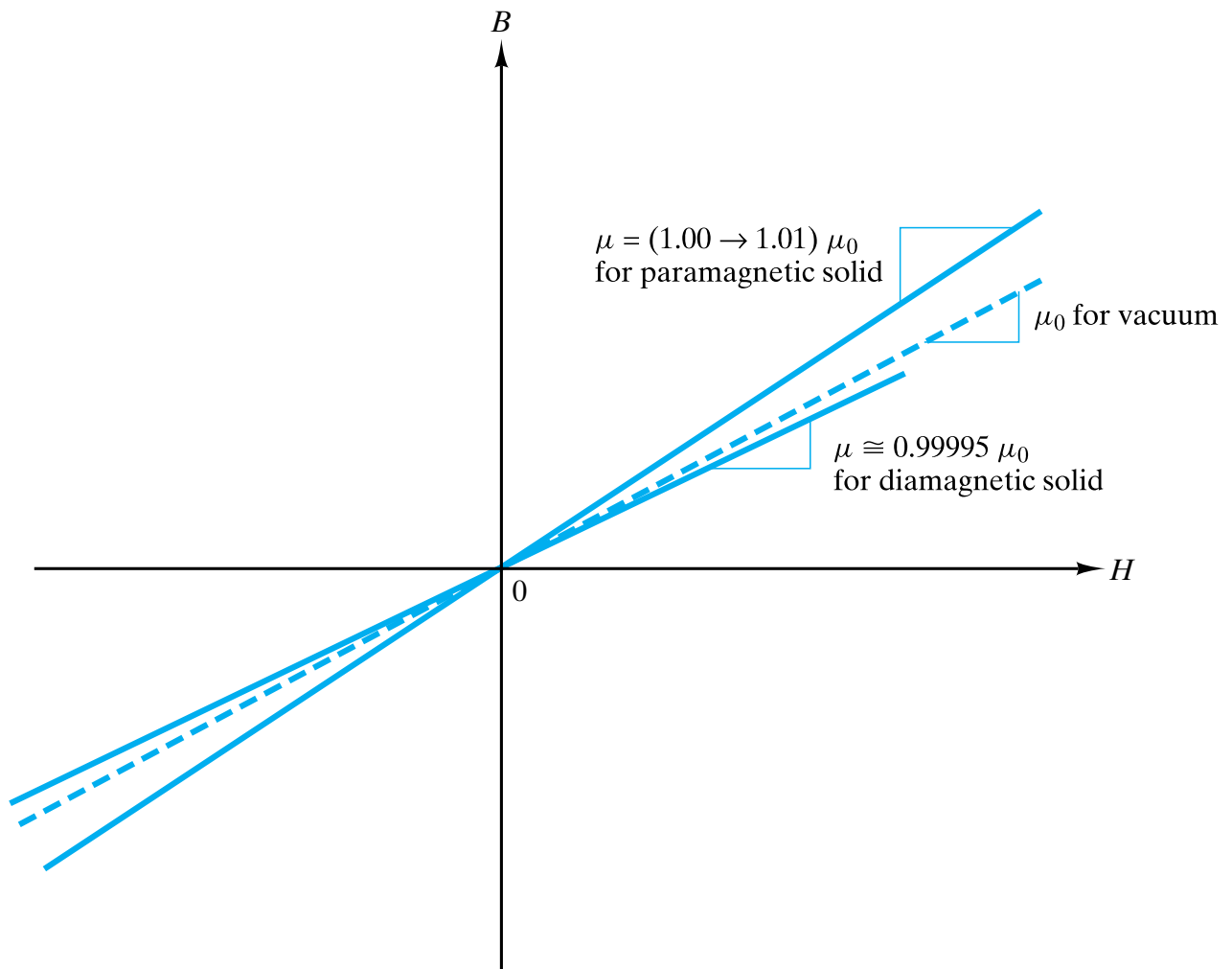


Figure 18-4 Comparison of diamagnetism and paramagnetism on a plot of induction (B) versus magnetic field strength (H). Neither of these phenomena is of practical engineering importance due to the modest level of induction that can be generated.

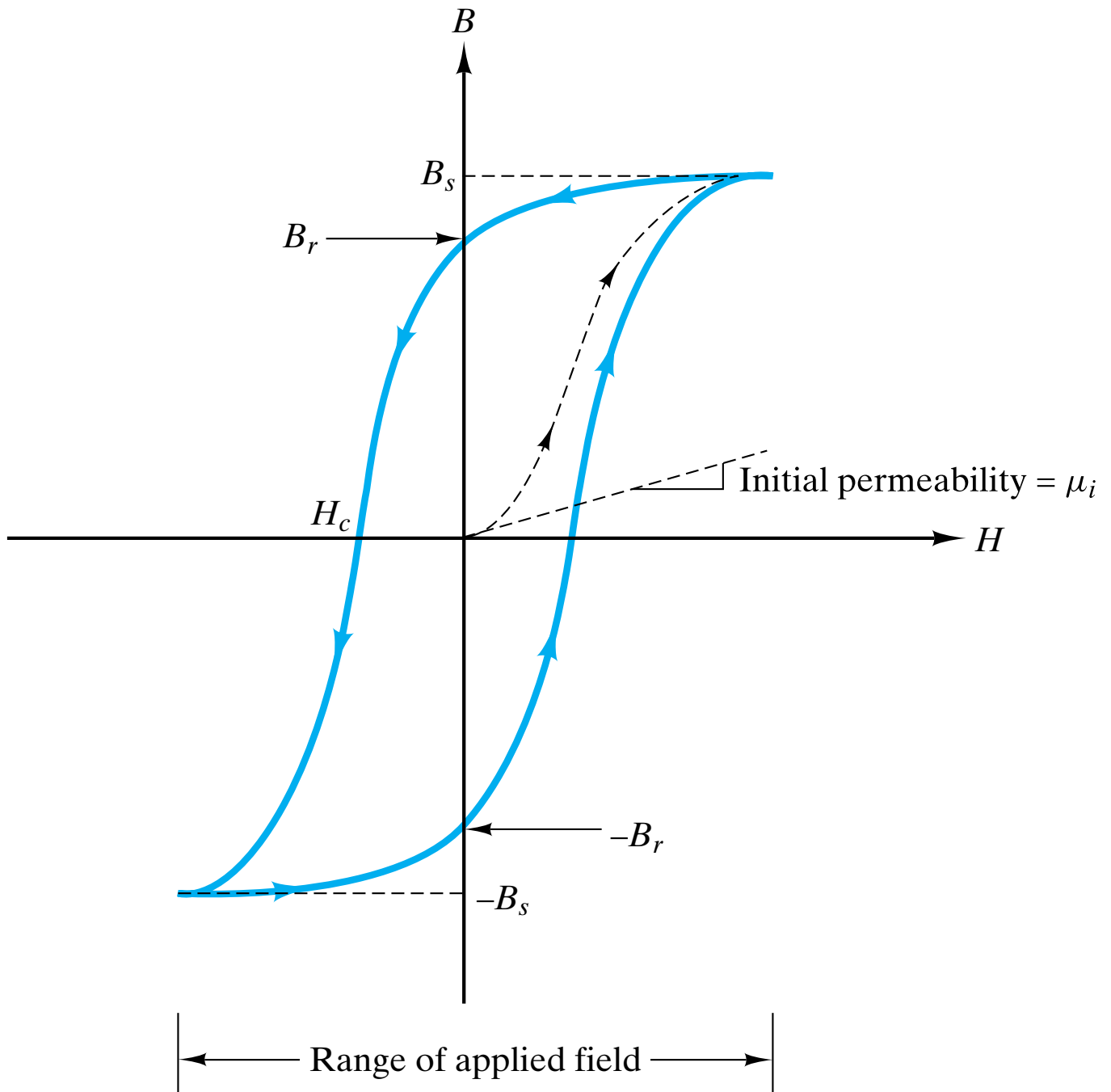


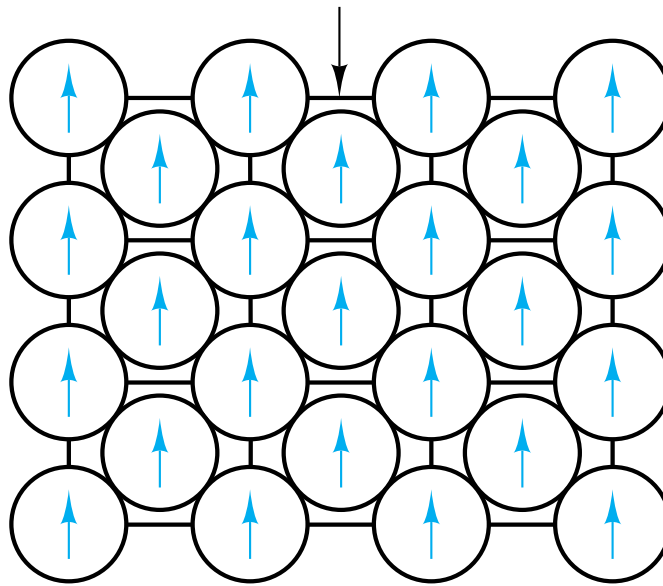
Figure 18-5 In contrast to Figure 18-4, the B - H plot for a ferromagnetic material indicates substantial utility for engineering applications. A large rise in B occurs during initial magnetization (shown by the dashed line). The induction reaches a large, “saturation” value (B_s) upon application of sufficient field strength. Much of that induction is retained upon removal of the field ($B_r =$ remanent induction). A coercive field (H_c) is required to reduce the induction to zero. By cycling the field strength through the range indicated, the B - H plot continuously follows the path shown as a solid line. This is known as a hysteresis loop.

Atomic number	Element	Electronic structure of 3d	Moment (μ_B)
21	Sc	\uparrow \square \square \square \square	1
22	Ti	\uparrow \uparrow \square \square \square	2
23	V	\uparrow \uparrow \uparrow \square \square	3
24	Cr	\uparrow \uparrow \uparrow \uparrow \uparrow	5
25	Mn	\uparrow \uparrow \uparrow \uparrow \uparrow	5
26	Fe	$\uparrow\downarrow$ \uparrow \uparrow \uparrow \uparrow	4
27	Co	$\uparrow\downarrow$ $\uparrow\downarrow$ \uparrow \uparrow \uparrow	3
28	Ni	$\uparrow\downarrow$ $\uparrow\downarrow$ $\uparrow\downarrow$ \uparrow \uparrow	2
29	Cu	$\uparrow\downarrow$ $\uparrow\downarrow$ $\uparrow\downarrow$ $\uparrow\downarrow$ $\uparrow\downarrow$	0

\uparrow = electronic spin orientation

Figure 18-6 *The electronic structure of the 3d orbital for transition metals. Unpaired electrons contribute to the magnetic nature of these metals.*

(110) plane in bcc α - Fe



Each $\uparrow = 4\mu_B$

Figure 18-7 *The alignment of magnetic moments for adjacent atoms leads to the large net magnetic moment (and B_s on a B - H plot) for the bulk solid. The example here is pure bcc iron at room temperature.*

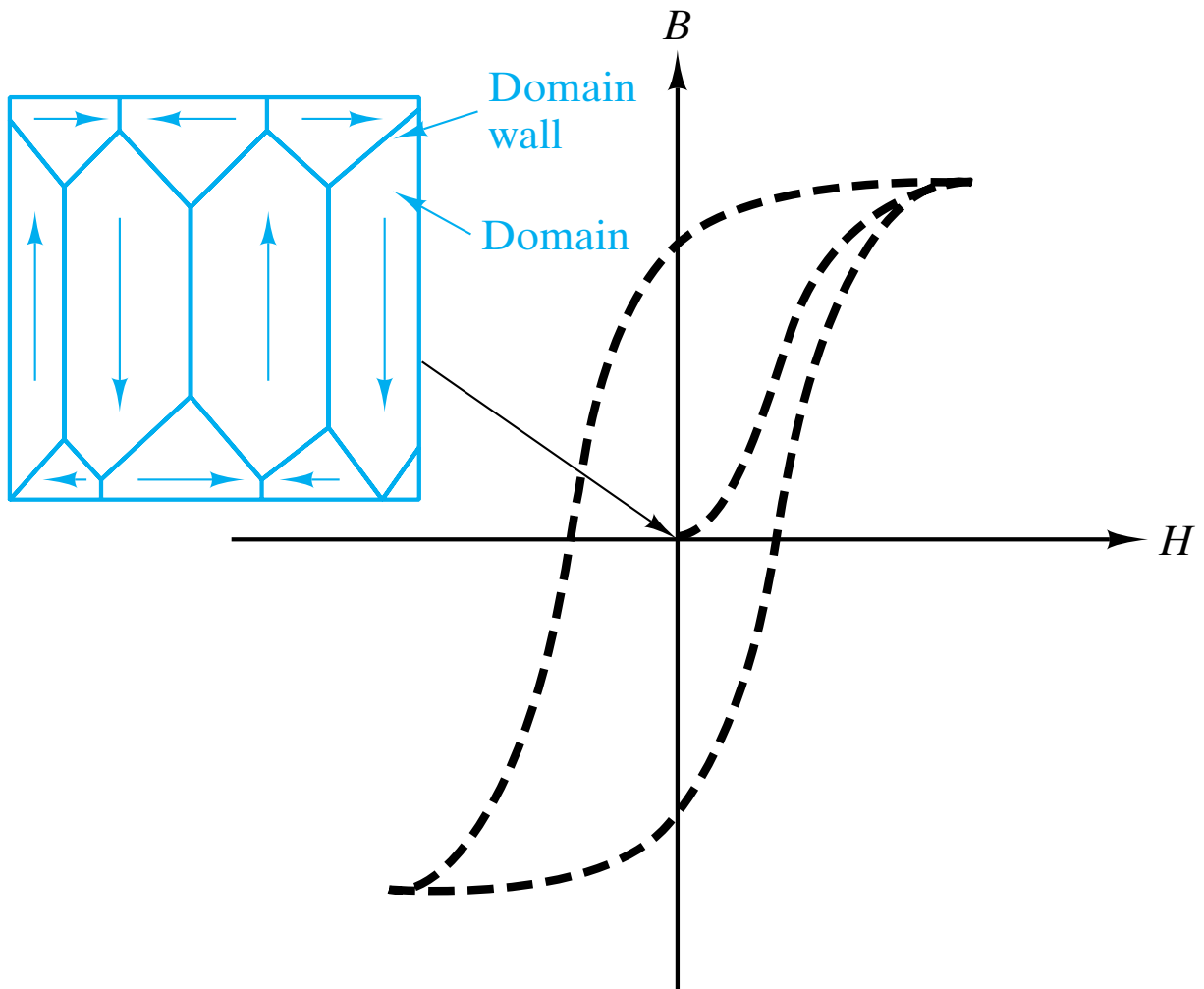


Figure 18-8 *The domain structure of an unmagnetized iron crystal gives a net $B = 0$ even though individual domains have the large magnetic moment indicated by Figure 18-7.*

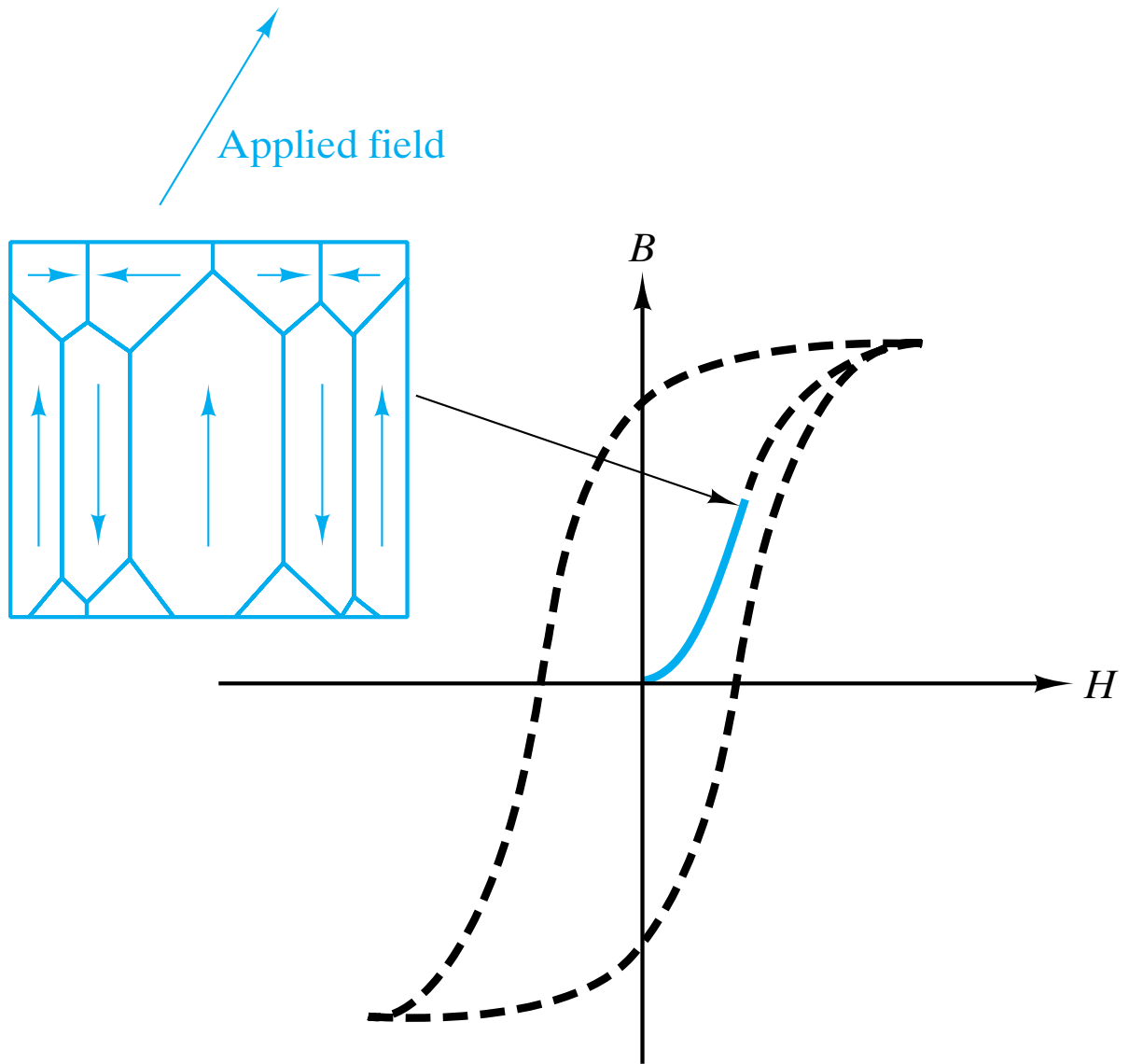


Figure 18-9 *The sharp rise in B during initial magnetization is due to domain growth.*

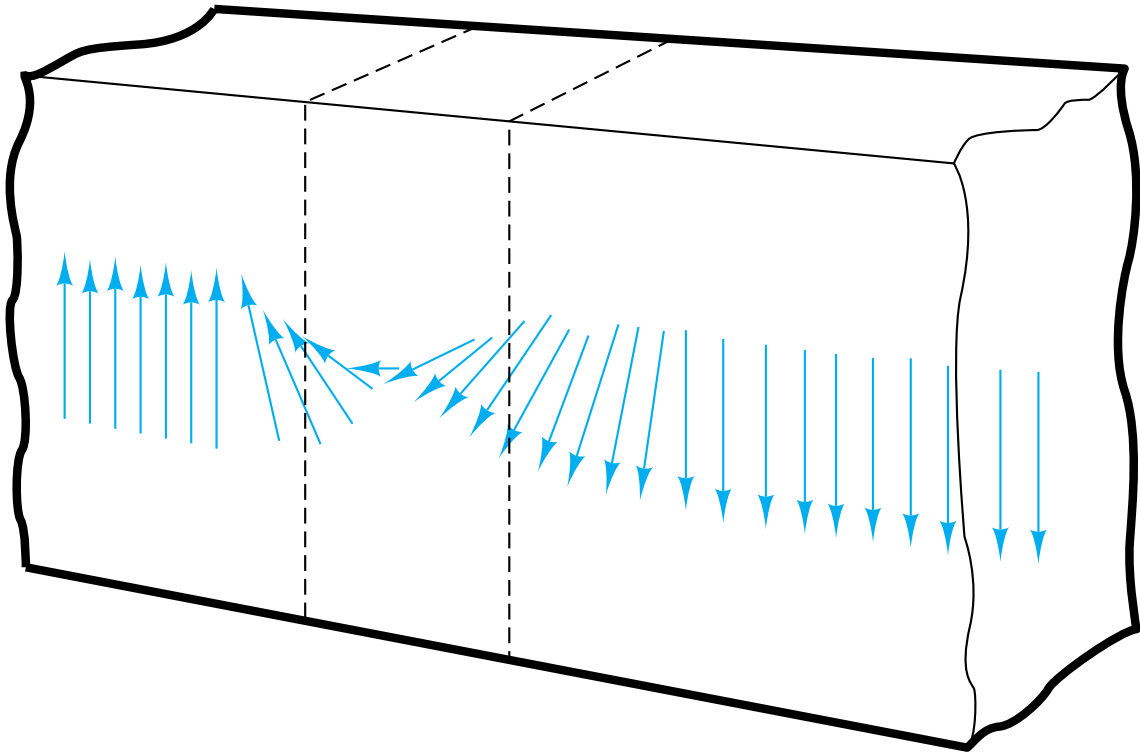


Figure 18-10 *The domain, or Bloch, wall is a narrow region in which atomic moments change orientation by 180° . Domain wall motion (implied in Figures 18-8 and 18-9) simply involves a shift in this reorientation region. No atomic migration is required.*

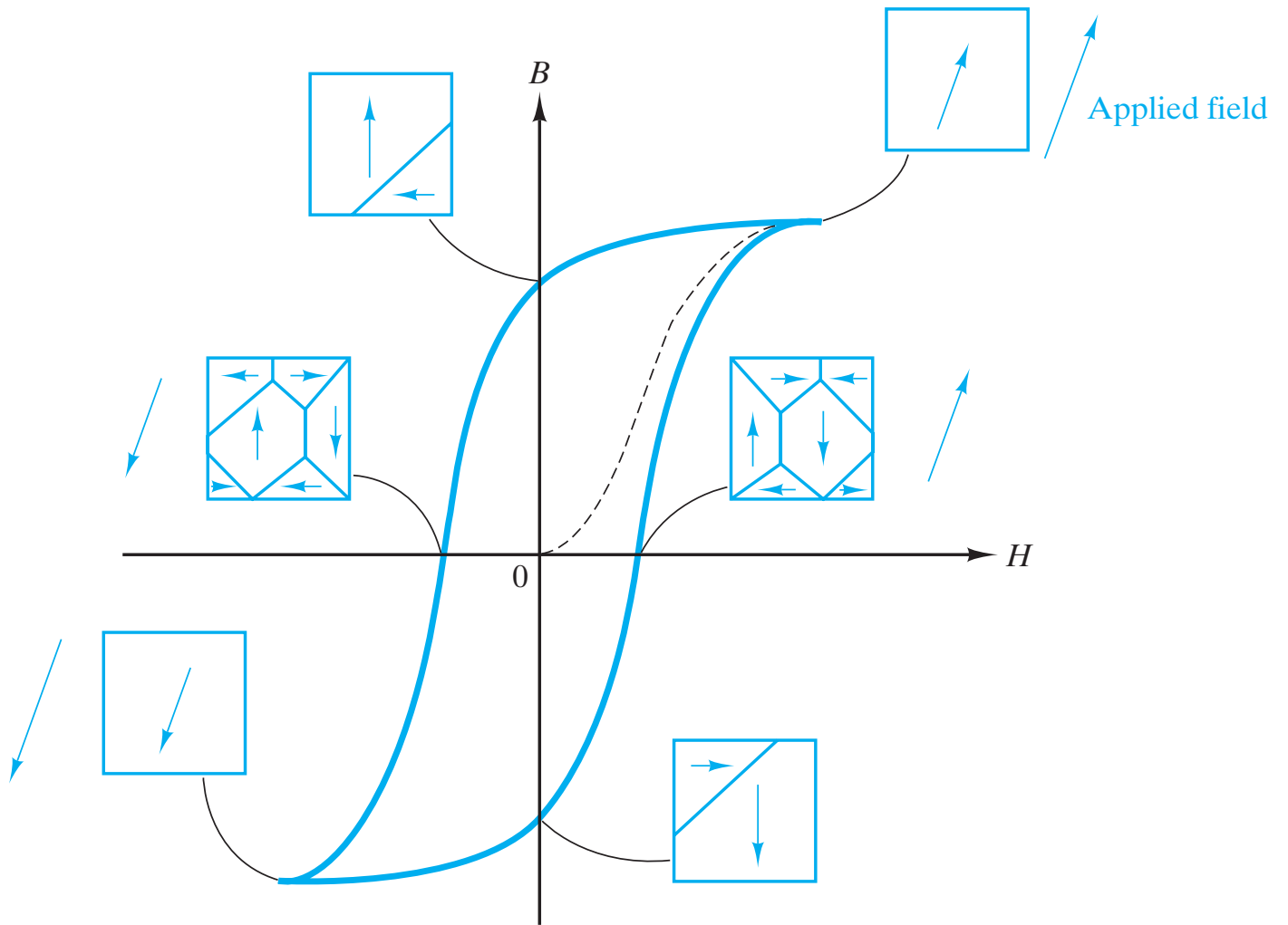
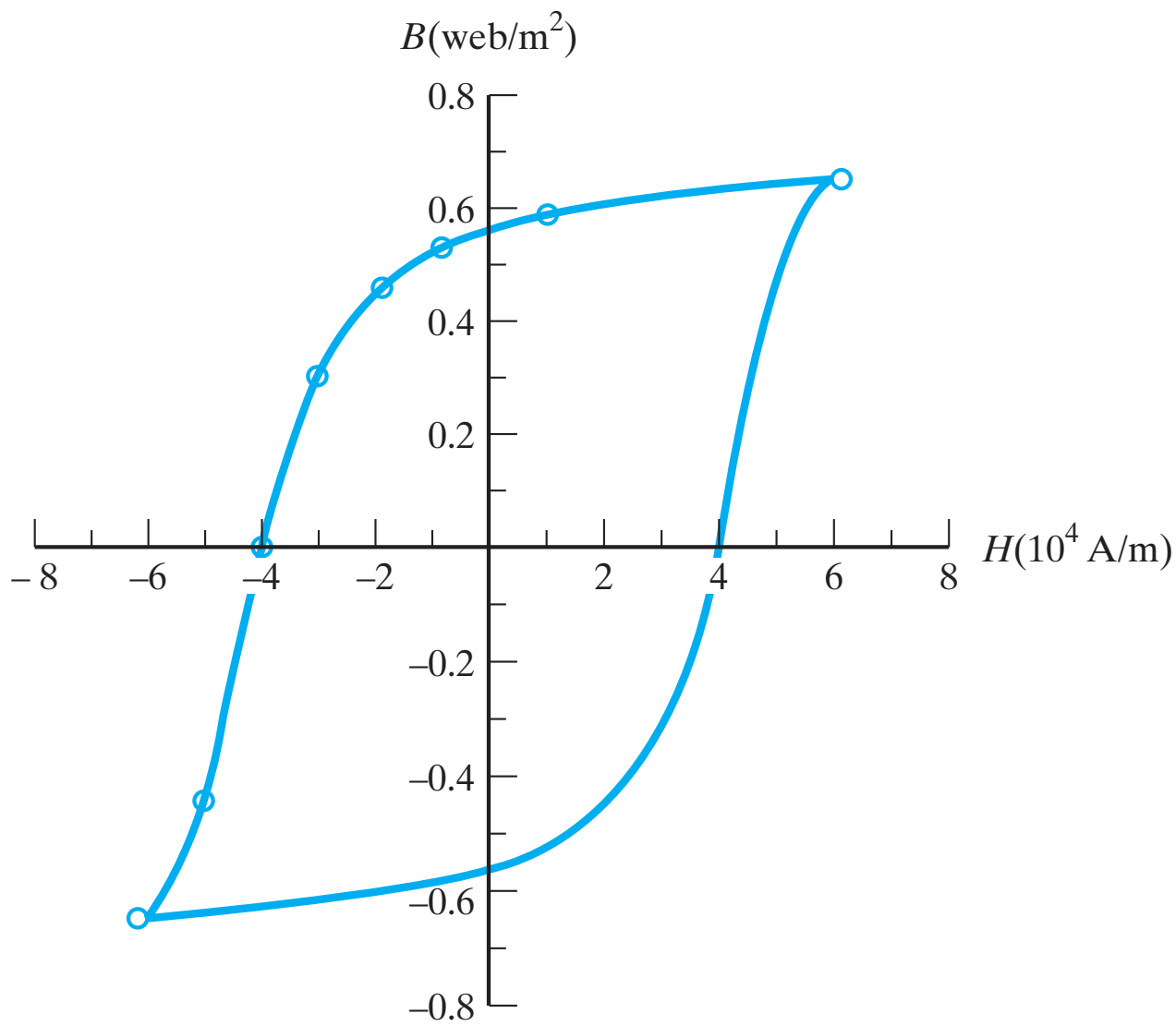


Figure 18-11 Summary of domain microstructures during the course of a ferromagnetic hysteresis loop.



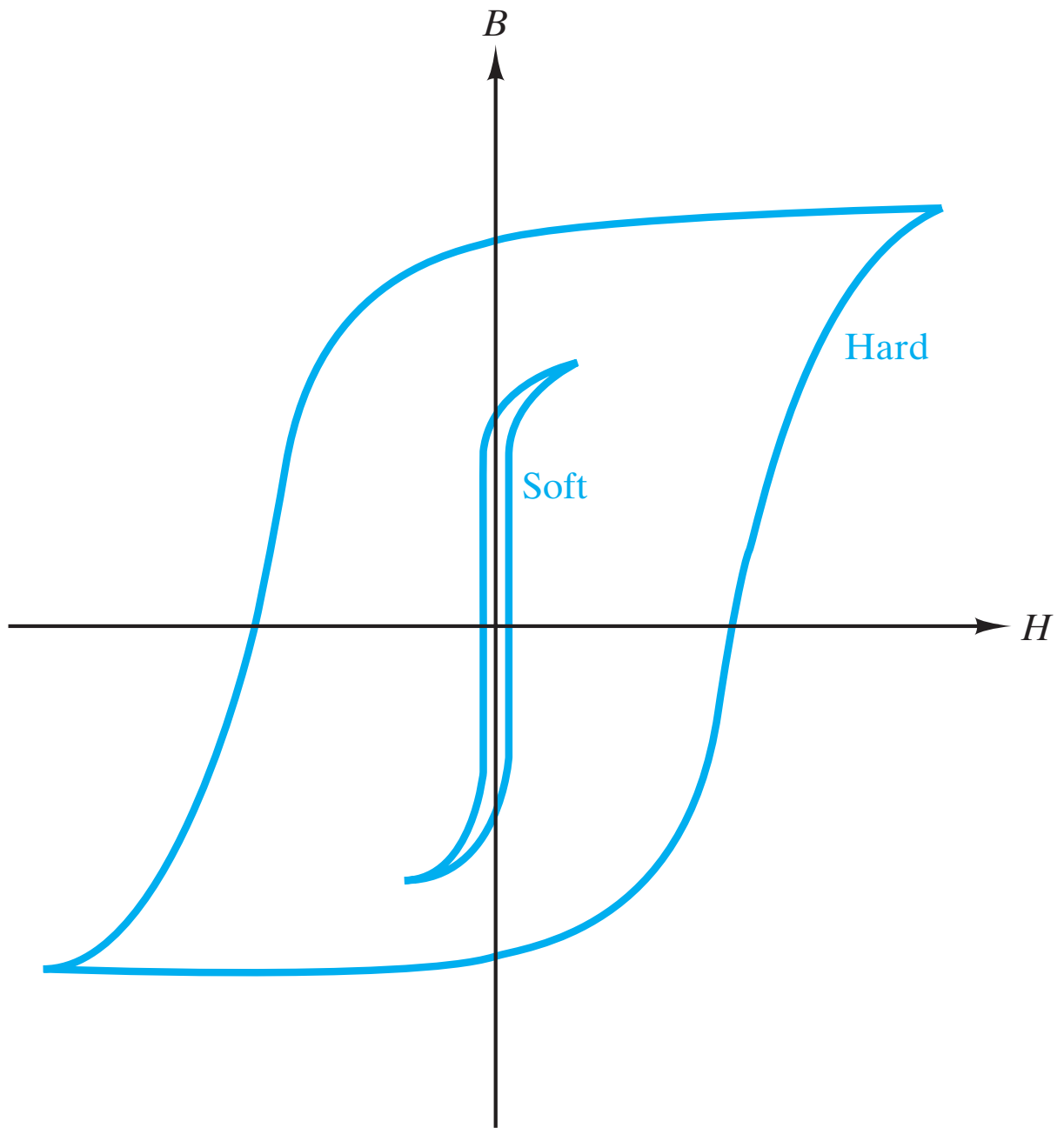
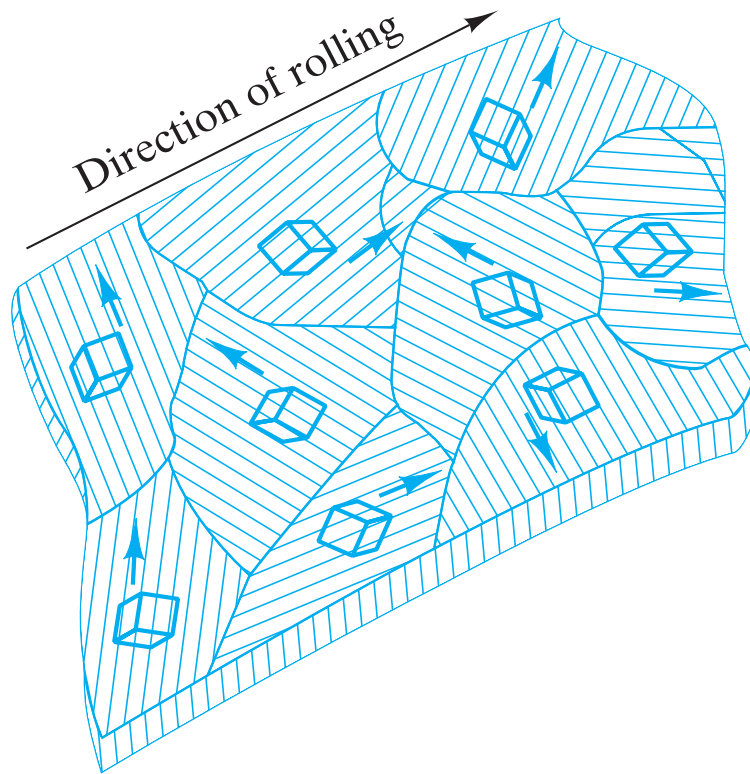
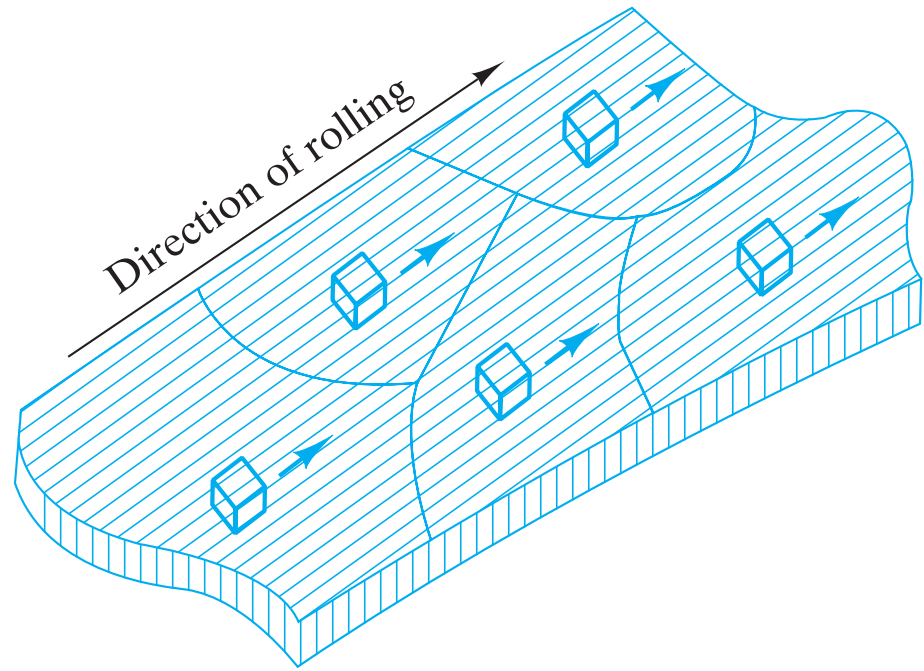


Figure 18-12 Comparison of typical hysteresis loops for “soft” and “hard” magnets.



(a) Random



(b) Textured

Figure 18-13 A comparison of (a) random and (b) textured (with preferred orientation) microstructures in polycrystalline iron-silicon alloy sheets. The preferred orientation is the result of cold rolling. The small cubes represent the orientation (but not the size) of unit cells in each grain's crystal structure. The preferred orientation (b) is termed $(100)[001]$, corresponding to the plane and direction of the unit cells relative to the sheet geometry. Figure 18-14 shows how the textured microstructure takes advantage of the crystallographic anisotropy of magnetic properties. (From R. M. Rose, L. A. Shepard, and J. Wulff, *The Structure and Properties of Materials, Vol. 4: Electronic Properties*, John Wiley & Sons, Inc., New York, 1966.)

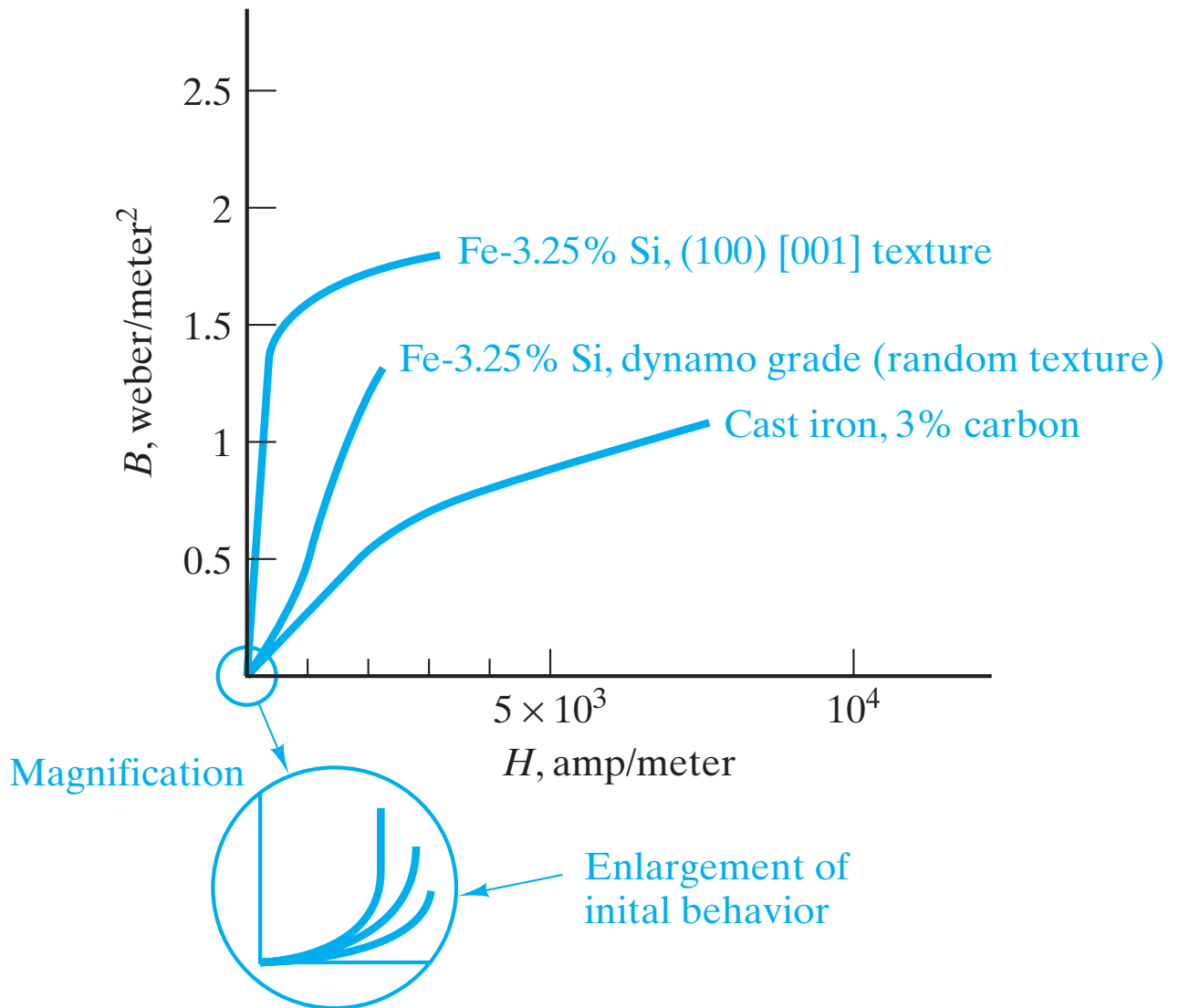


Figure 18-14 A comparison of initial magnetization for three ferrous alloys. The silicon addition increases magnetic permeability and, consequently, B_s . Preferred orientation, or texturing, increases initial magnetization substantially (see Figure 18-13). (From R. M. Rose, L. A. Shepard, and J. Wulff, *The Structure and Properties of Materials, Vol. 4: Electronic Properties*, John Wiley & Sons, Inc., New York, 1966.)

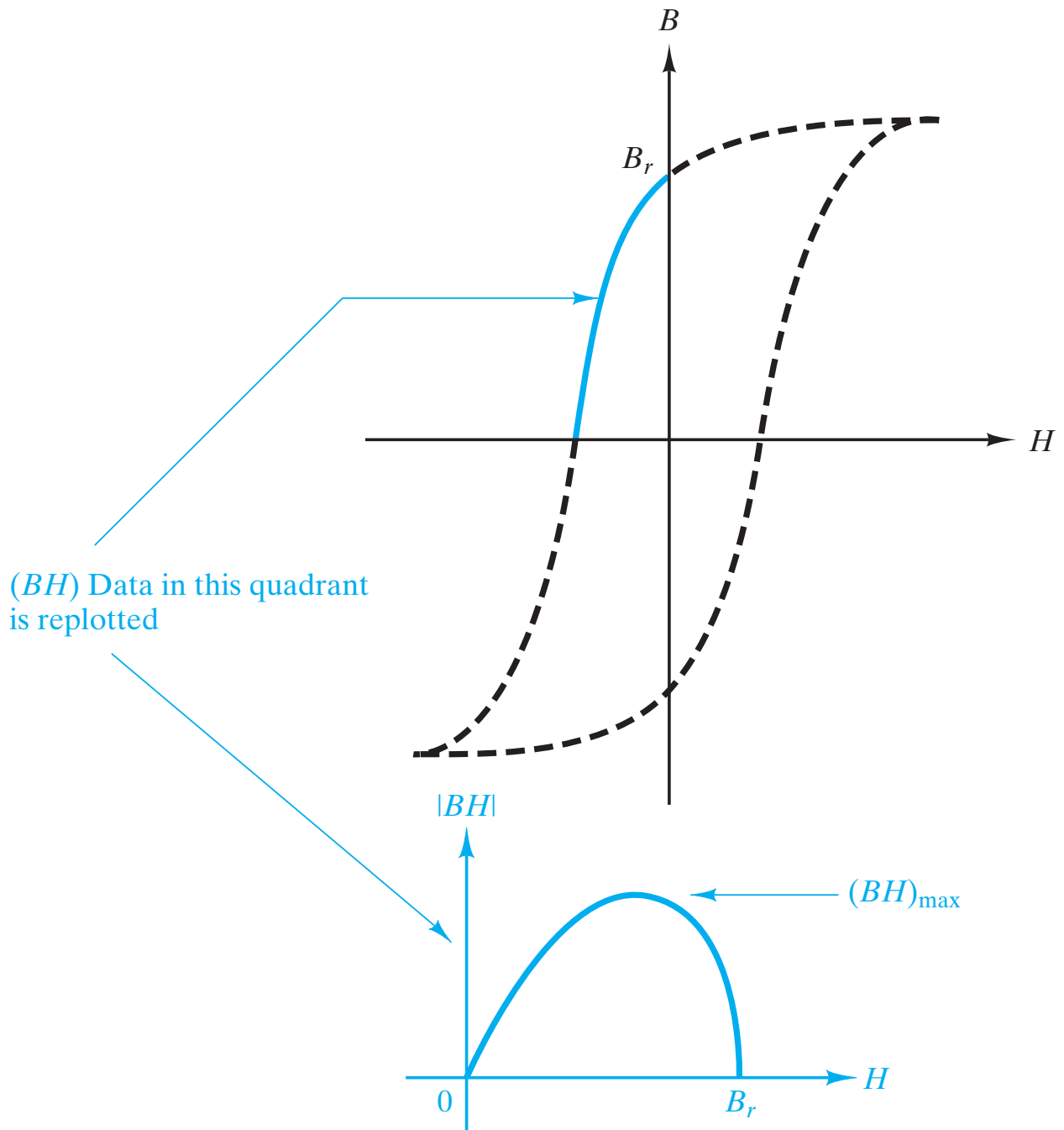
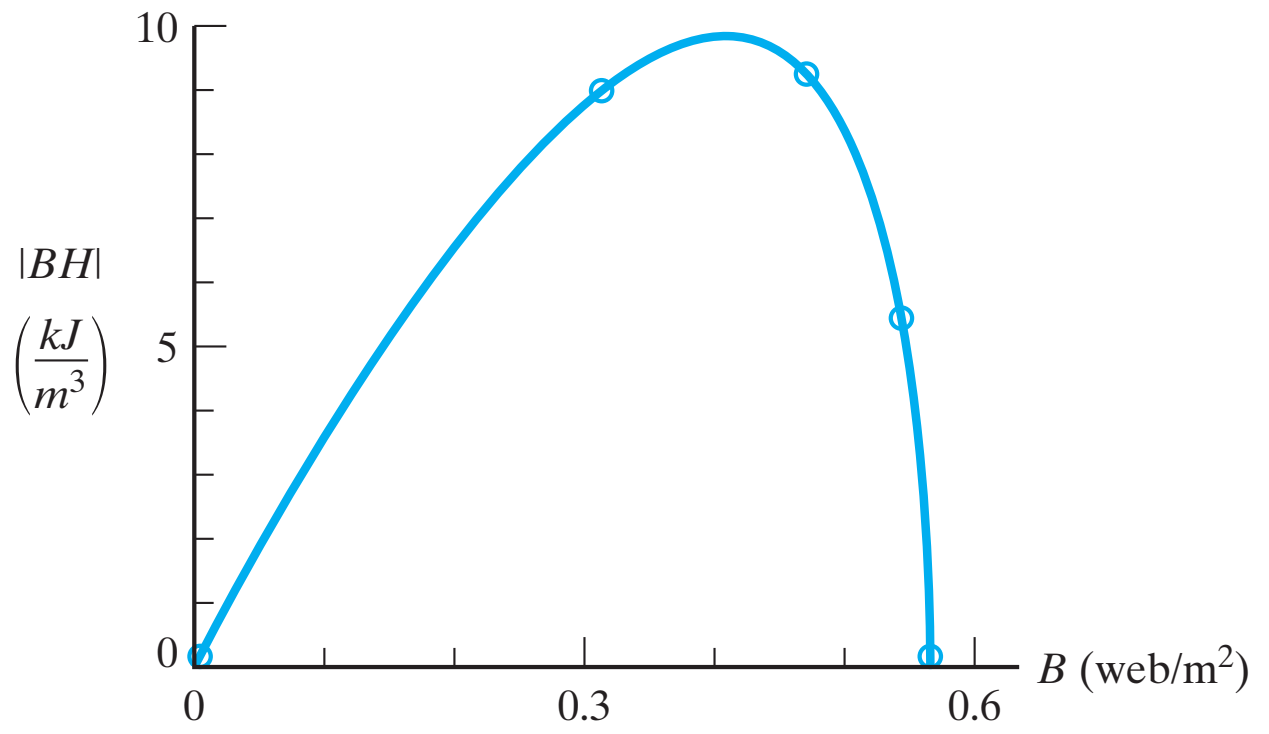


Figure 18-15 Replotting data in the “demagnetization quadrant” of the hysteresis loop demonstrates a maximum value of the $|BH|$ product, $(BH)_{\max}$. This quantity is a convenient measure of the “power” of permanent magnets. Table 18.3 gives $(BH)_{\max}$ for various hard magnets.



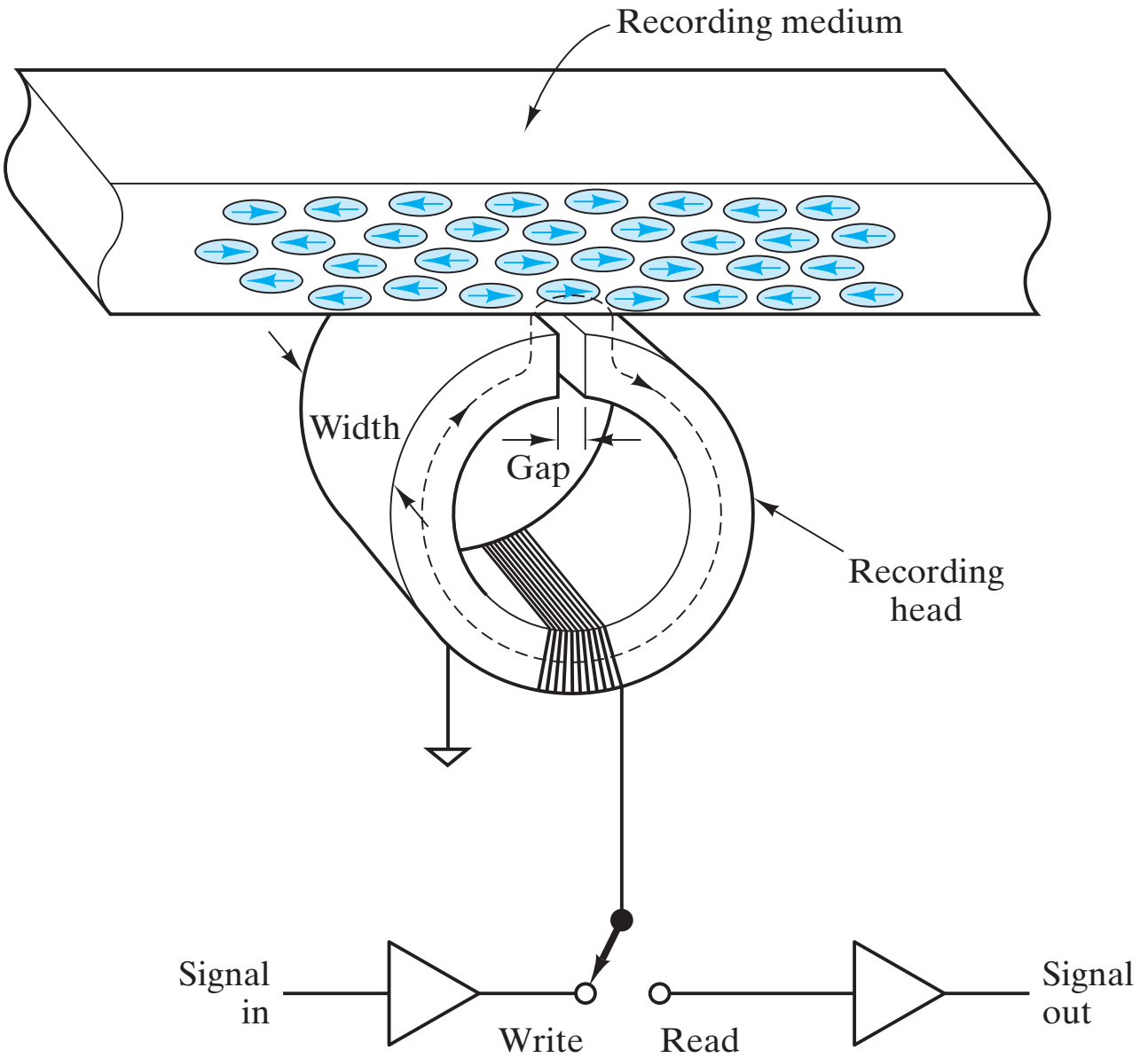


Figure 18-16 Schematic illustration of magnetic storage and retrieval using a recording medium composed of needlelike particles of $\gamma\text{-Fe}_2\text{O}_3$. (From J. U. Lemke, *MRS Bulletin*, 15, 31 [1990].)

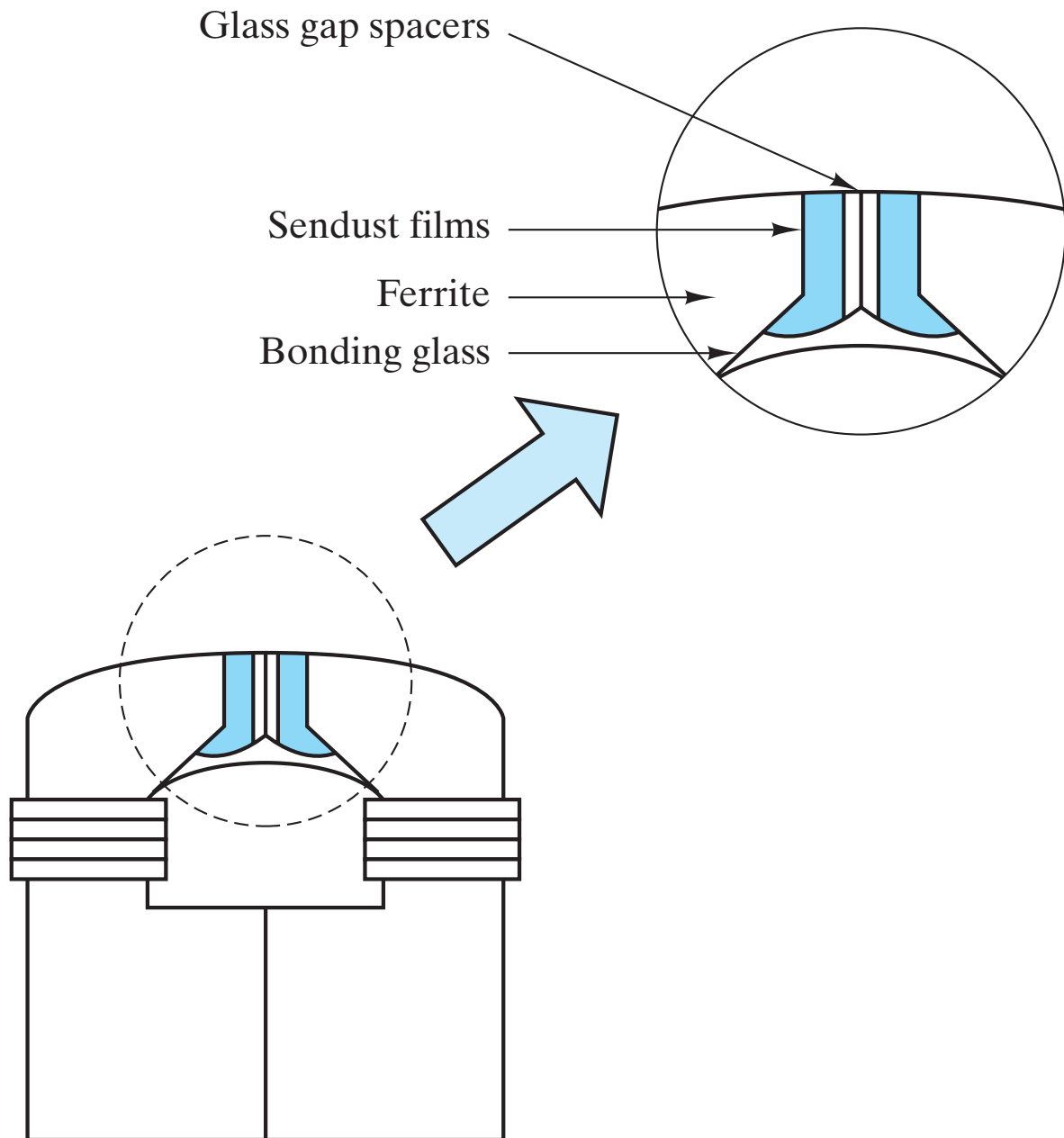


Figure 18-17 Schematic illustration of a thin film of a metal alloy, Sendust (FeAlSi), on the pole faces of the ferrite recording head in a metal-in-gap or MiG design. (From A. S. Hoagland and J. E. Monson, *Digital Magnetic Recording*, 2nd ed., Wiley-Interscience, New York, 1991.)

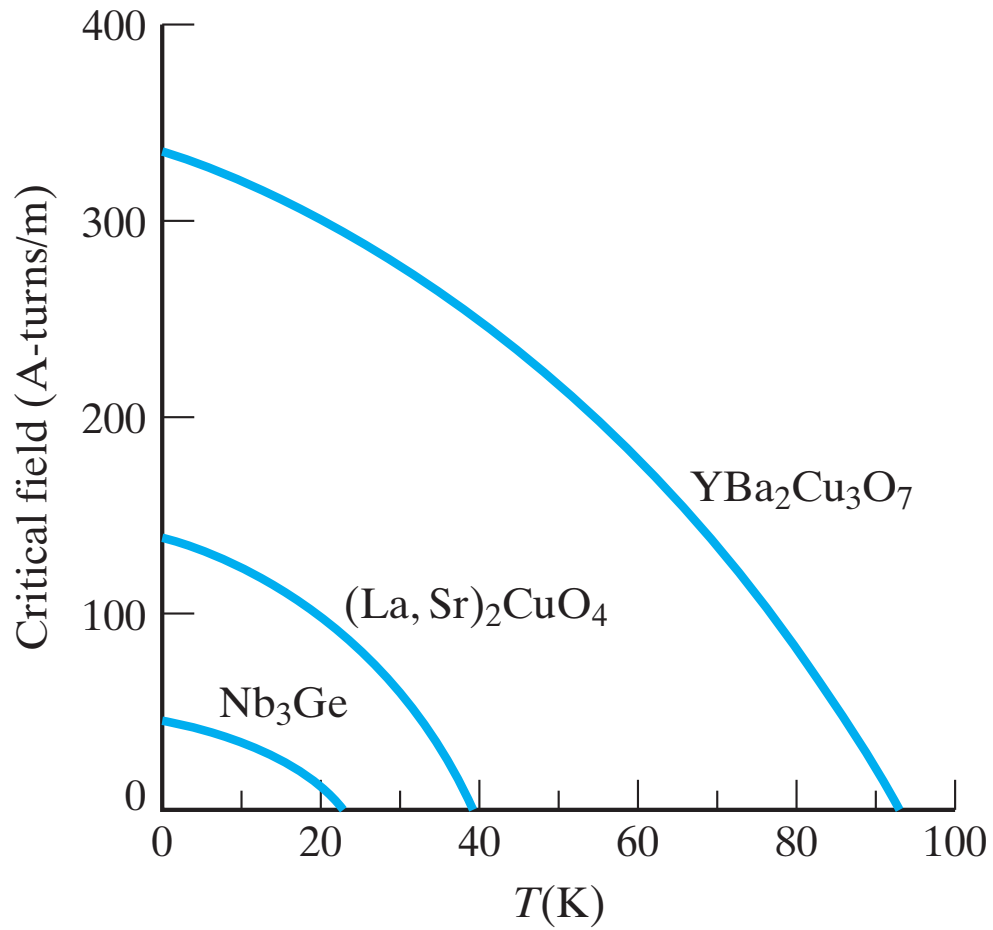


Figure 18-18 Comparison of the critical magnetic field versus temperature for a metallic superconductor (Nb_3Ge) and two ceramic superconductors.